

Catalysis Science & Technology

Accepted Manuscript

This article can be cited before page numbers have been issued, to do this please use: L. Popp and P. Schühle, *Catal. Sci. Technol.*, 2026, DOI: 10.1039/D6CY00216A.



This is an Accepted Manuscript, which has been through the Royal Society of Chemistry peer review process and has been accepted for publication.

Accepted Manuscripts are published online shortly after acceptance, before technical editing, formatting and proof reading. Using this free service, authors can make their results available to the community, in citable form, before we publish the edited article. We will replace this Accepted Manuscript with the edited and formatted Advance Article as soon as it is available.

You can find more information about Accepted Manuscripts in the [Information for Authors](#).

Please note that technical editing may introduce minor changes to the text and/or graphics, which may alter content. The journal's standard [Terms & Conditions](#) and the [Ethical guidelines](#) still apply. In no event shall the Royal Society of Chemistry be held responsible for any errors or omissions in this Accepted Manuscript or any consequences arising from the use of any information it contains.

ARTICLE

Nickel catalysts in the hydrogenation of benzyltoluene using impure hydrogen streams

Lukas Popp, Patrick Schühle

Received 00th January 20xx,
Accepted 00th January 20xx

DOI: 10.1039/x0xx00000x

Biomass-derived hydrogen is frequently contaminated with CO and CO₂, which limits its direct utilization in downstream applications. Cyclic hydrogenation/dehydrogenation of liquid organic hydrogen carriers (LOHCs) such as benzyltoluene (BT) provides a pathway to simultaneously store hydrogen and purify such “low-grade” hydrogen feeds. In this context, Ni-based catalysts are particularly attractive because they can hydrogenate aromatic systems under CO-containing atmospheres while representing a relatively cheap alternative to noble metal catalyst. Here, we systematically investigate BT hydrogenation over a commercial Ni/Al₂O₃/SiO₂ catalyst under process-relevant LOHC conditions (T = 170–230 °C, p = 10–50 bar) in the presence of CO (0–6 %) and demonstrate that BT conversion remains feasible even at high CO levels, while the hydrogenation rate decreases due to competitive CO adsorption. Time-resolved analysis of both gas- and liquid-phase compositions further reveals CO methanation during BT hydrogenation, indicating that both reactions proceed in parallel while competing for active sites. By varying temperature and total pressure, the balance between BT hydrogenation and methanation can be steered, with 230 °C and 50 bar identified as the most favorable conditions for efficient BT hydrogenation under CO presence. In addition, introducing CO₂ at biomass-typical concentrations (30 vol%) shows that it likewise adsorbs competitively on Ni and is also converted to methane. Collectively, these results highlight Ni-based catalysts as a robust catalyst for mixed-gas hydrogenation and LOHC-enabled purification/storage of biogenic hydrogen, while underscoring an inherent trade-off between competitive (co-)methanation, that consumes a fraction of hydrogen as CH₄ that cannot be recovered upon LOHC dehydrogenation, yet constitutes an energy-dense coproduct stream that may be valorized

Introduction

The conversion of waste-derived biomass into hydrogen is emerging as a pivotal strategy in the transition to a sustainable, circular energy economy^{1–3}. This approach leverages biogenic residues, such as agricultural by-products, organic waste, sewage sludge, and forestry residues, thereby mitigating the competition with food production and contributing to carbon-neutral hydrogen production^{4–7}.

The gas mixture resulting from biomass conversion e.g. by gasification predominantly comprises hydrogen (H₂), carbon monoxide (CO), carbon dioxide (CO₂), methane (CH₄), and nitrogen (N₂)^{8–10}. While hydrogen is the desired energy carrier, the presence of these impurities poses significant challenges for its direct utilization in e.g., fuel cell applications. Carbon monoxide is a potent catalyst poison, even at low concentrations, leading to irreversible deactivation of platinum- or nickel-based catalysts in membrane fuel cells (PEMFC and HEMFC)^{11–14}. Carbon dioxide acts on one hand as an inert diluent, reducing the hydrogen partial pressure and

thereby decreasing the electrochemical conversion efficiency^{15,16}. On the other hand certain catalysts can promote the formation of CO from CO₂ in the presence of hydrogen, for example via the reverse water–gas shift reaction¹⁷. Methane, formed during incomplete reforming or at low temperatures, increases the calorific value of the gas but is unsuitable for direct fuel cell utilization and requires additional processing, such as steam reforming, to release usable hydrogen¹⁰. Nitrogen, introduced during e.g. air-based gasification, significantly dilutes the syngas and does not participate in electrochemical reactions, further reducing the energy density per unit volume and complicating downstream processing^{18,19}. Conventional hydrogen purification methods such as pressure swing adsorption (PSA), cryogenic separation, and chemical scrubbing are energy-intensive and costly^{20,21}. PSA alone typically cannot achieve PEM fuel cell–grade hydrogen purity (>99. %) and therefore, requires additional purification steps^{22–24}. Cryogenic separation demands substantial refrigeration energy, while chemical scrubbing involves continuous reagent consumption and added operational complexity²⁵. These technologies also perform poorly under fluctuating gas compositions typical of biomass-derived streams^{26,27}. High capital and operating costs, along with multi-stage process integration, limit their suitability for small- and medium-scale decentralized biomass-to-hydrogen applications^{22,24}. Hydrogen purification can

^a Institute of Chemical Reaction Engineering, Friedrich-Alexander-Universität^b Erlangen-Nürnberg, 91058 Erlangen, Germany

Supplementary Information available: [details of any supplementary information available should be included here]. See DOI: 10.1039/x0xx00000x



also be accomplished through cyclic hydrogenation/dehydrogenation of unsaturated hydrocarbons. In this process, hydrogen present in a mixed gas stream is selectively bound covalently to a liquid carrier via catalytic hydrogenation, while accompanying impurities are removed through the gas phase (see Figure 1). Subsequent catalytic dehydrogenation enables the recovery of hydrogen in high purity, and the carrier liquid is regenerated for repeated use forming the cyclic process. Liquid organic hydrogen carriers (LOHCs), so far investigated for hydrogen storage and transportation, can consequently also be applied to accomplish hydrogen purification. Among these organic carriers, benzyltoluene (BT) has emerged as an especially promising substance, due to its high hydrogen storage capacity, favourable hazard profile, wide liquid-phase temperature range and commercial availability in large scales. Hydrogen-lean BT (H0-BT) is converted to its hydrogen rich form perhydro-benzyltoluene (H12-BT) via catalytic hydrogenation at 150–180 °C and 20–30 bar hydrogen pressure^{28,29}. Subsequent catalytic dehydrogenation at 280–300 °C near atmospheric pressure enables the recovery of hydrogen in high purity, while the benzyltoluene carrier is regenerated for repeated use^{30–32}.

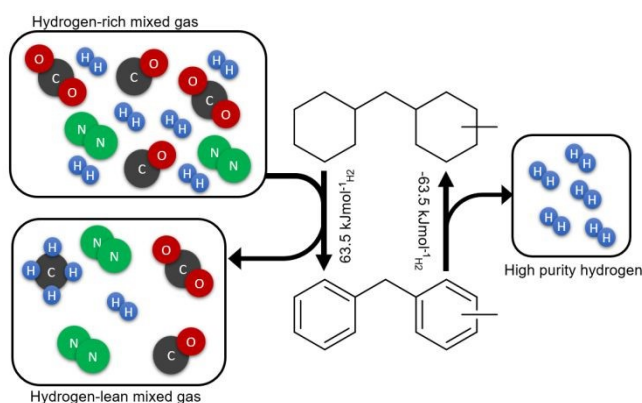
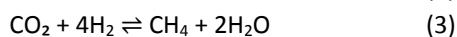
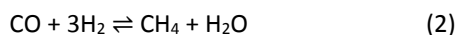
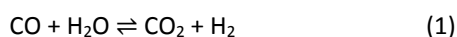


Figure 1 (De-)hydrogenation cycle to purify hydrogen with the use of Benzyltoluene as a purification liquid.

In direct hydrogenation of liquid carriers with impure hydrogen (mixed gas hydrogenation), the gas phase contains H₂, CO, and CO₂, which can undergo the (reverse) water–gas shift reaction (1) and methanation reactions (2,3) in parallel³³.



These processes alter the hydrogen partial pressure and gas composition near the liquid–gas interface, thereby influencing hydrogen availability for the LOHC hydrogenation. Depending on operating conditions and catalyst, the extent of these gas-phase conversions can significantly affect the overall hydrogen utilization efficiency^{34,35}. Understanding these coupled gas-phase reactions is therefore essential for optimizing the performance and selectivity of mixed-gas LOHC hydrogenation systems. The hydrogenation

process is typically catalysed by noble metals like Pt or Pd, due to their superior activity and selectivity^{32,36,37}. However, these noble metal catalysts are highly susceptible to impurities—especially CO—which strongly adsorb on active sites and severely reduce hydrogenation efficiency. Recent investigations on LOHC systems by Jorschick *et al.* demonstrated that Pd/Al₂O₃ maintains BT hydrogenation activity in gas mixtures containing low amounts of CO and CO₂, while Pt centres are completely poisoned under applied conditions³⁸. Seitz *et al.* found that phosphate modification of Pd/Al₂O₃ significantly enhances catalytic activity and stability in aromatic hydrogenation under CO-contaminated hydrogen, attributing this to the expression of poisoning-resistant Pd sites due to small particle diameters³⁹. Nickel represents a valid alternative to Pd for hydrogenation catalysts: economically, Ni is orders of magnitude less expensive than Pd, and catalytically, Ni-based catalyst have demonstrated competitive activity in the hydrogenation of aromatic compounds⁴⁰. Moreover, when used in tandem with noble metals, these systems exhibit enhanced resistance to CO poisoning while maintaining high hydrogenation performance⁴¹. Regarding the performance under CO-containing atmosphere liquid-phase naphthalene hydrogenation was investigated by Sekine *et al.* over a supported Ni catalyst, showing that Ni retains measurable aromatic hydrogenation activity despite CO adsorption and concurrent CO hydrogenation⁴². Additionally, Le *et al.* evaluated Ni/SiO₂ catalysts using benzene hydrogenation alongside CO methanation, to assess Ni functionality for aromatic saturation alongside CO conversion under process-relevant conditions⁴³.

In this study, the hydrogenation of benzyltoluene in the presence of CO- and CO₂ containing hydrogen gas mixtures is demonstrated by using a commercial nickel-based catalyst. The effects of temperature, total pressure, and the partial pressures of the aforementioned impurities on H0-BT conversion, selectivity and stability are discussed. The progression of gas and liquid phase composition is monitored to enable a comprehensive understanding of the parallel reaction pathways.

Experimental

Materials

All chemicals were commercially sourced and utilized without additional purification. A nickel, silica and alu-mina extrudate (Ni/Al₂O₃/SiO₂, loading 50 wt%, Clarinat[®]) was used as the hydrogenation catalyst. H0-Benzyltoluene (Hydrogenious Technologies[®]) is used as the LOHC. For the hydrogenation experiments, hydrogen (H₂, Air Liquide, 99.99%), a carbon monoxide/hydrogen mixture (2% CO in H₂, Air Liquide; 99.99%), carbon dioxide (CO₂, Air Liquide, 99.99%), nitrogen (N₂, Air Liquide, 99.99%) and argon (Ar, Air Liquide, 99.99%) were used as reaction gases. Liquid samples were dissolved in acetone (C₃H₆O, ≥99.8% Merck KGaA) for further analysis. Chemicals used for catalyst characterization are mentioned below.



demonstrate a catalyst concept with practical potential for mixed-gas hydrogenation rather than to develop or optimize a model catalyst. For this reason, the characterization of the commercial

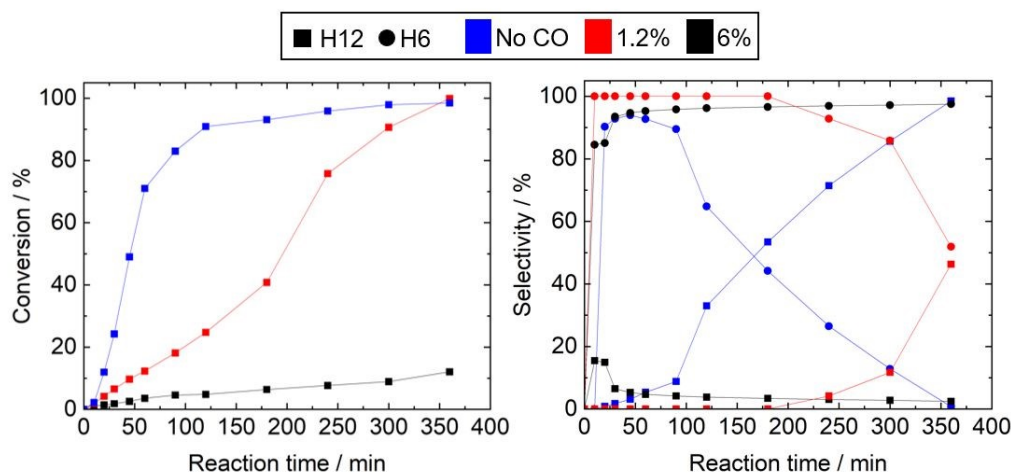


Figure 2 Conversion (left) and selectivity (right) of Benzyltoluene hydrogenation using a commercial Nickel catalyst without CO impurities (blue), with 1.2 % CO-gas fraction (red) as well as 6 % CO-gas fraction (black)(reaction conditions: Ni/BT ratio 0.045, $m_{BT} = 100$ g, $T = 170$ °C, $t = 6$ h; $p = 50$ bar)

Catalyst Characterisation

The crystal structure of the catalyst was investigated using powder X-ray diffraction (XRD). The measurements were carried out in angles of $10\text{--}90^\circ 2\theta$, a scanning speed of $0.02^\circ/\text{s}$, a step size of 0.015° and 100 s time per step on a X'Pert Pro by Malven Panalytcs. Cu-K α was used as the radiation source and X'Celerator as the detector. The data was processed utilizing X'Pert Highscore Plus and compared to simulated reflexes from the inorganic crystal structure database (ICSD). Elemental composition of the catalysts was measured via inductively coupled plasma-optical emission spectroscopy (ICP-OES). Approximately 100 mg of the samples were dissolved using microwave-assisted digestion at 220 °C in a solution containing HCl (32 %; Merck KGaA), HNO $_3$ (65 %, Merck KGaA) and HF (40 %Merck KGaA) (6:2:2 ml). The solutions were measured in an ICP-OES Ciros CCD from Spectro Analytical Instruments GmbH. The instrument was calibrated using standard Nickel containing solutions (Nickel ICP standard, based on nickel(II) nitrate; Merck KGaA). Three consecutive measurements of the dissolved samples were carried out, and an average value was calculated. The surface area, as well as the pore volume of the catalysts were determined by N $_2$ -Sorption on a Quantachrome Quadrasorb SI-MP-8. The samples were degassed at approximately 2×10^{-5} bar for 12 h at 250 °C. The relevant values were determined applying the Brunauer-Emmett-Teller (BET) theory. H $_2$ temperature-programmed reduction (H $_2$ -TPR) was performed on a Thermo Scientific TPDRO 1100 instrument (Thermo Electron Corporation). During the measurement, the sample was heated to a final temperature of 600 °C at a rate of 5 °C min^{-1} under a hydrogen flow of 20 $\text{cm}^3 \text{min}^{-1}$.

As this work aimed to assess the effect of CO on H $_0$ -BT hydrogenation in an industrially relevant system, a commercially available technical nickel catalyst was deliberately chosen to

catalyst was intentionally restricted to XRD, ICP-OES, N $_2$ physisorption and H $_2$ -TPR. These methods were considered sufficient to identify the crystalline phases, determine the bulk Ni content, describe the textural properties as well as guarantee a reduced and active Ni at Reaction condition which deemed relevant for reproducibility and comparison of catalytic results. A more detailed analysis of morphology, dispersion, and metal-support interaction by methods such as XPS, TEM or in situ DRIFT measurements was beyond the scope of the present study. Notably, in depth characterization of supported Ni-catalyst on Al $_2$ O $_3$ and SiO $_2$ is intensively reported in literature, whereas activity loss due to sintering, coking or phase changes are recorded at temperatures >300 °C^{44–49}.

Hydrogenation Experiments

Hydrogenation experiments were carried out in a 300 mL batch autoclave (Parr type 4566) equipped with a four-blade gas-inducing stirrer, an electric heating mantle, and a cooling coil connected to a cryostat (Huber Unichiller 022). The setup also included a type J thermocouple, a pressure recorder (Ashcroft type G2), and a process controller (Parr type 4875). A liquid sampling line fitted with a filter and needle valve (Nova Swiss) as well as a loop for continuous gas sampling were utilized. After the initial loading with 100 g H $_0$ -BT and Ni catalyst in a ratio $n_{Ni}:n_{H_0-BT}$ of 0.045 the reactor was sealed with a Kalrez $\text{\textcircled{C}}$ 4079 O-ring and the set-up was purged multiple times with Ar. The reactor was subsequently heated to a reaction temperature between $170\text{--}230$ °C, while stirring at 450 min^{-1} . After the desired temperature was reached, the liquid sample line was flushed with 1 ml reaction solution. 30 bar of the CO/H $_2$ mixture was introduced to reactor and 20 bar pure H $_2$ were added to reach the desired 50 bar hydrogenation pressure. Experiments were conducted in dead-end mode, maintaining constant H $_2$ pressure by continuously supplying H $_2$ to compensate



for its consumption during the reaction. The reaction was initiated by increasing the stirrer speed stepwise to 1200 min^{-1} , ensuring sufficient gas entrainment as well as mixing of the catalyst and the reaction fluids. The intervals for liquid and gas sampling as listed in table S1. In additional experiments 15 bar of the CO/H_2 mixture were replaced by 15 bar of either CO_2 or N_2 . This additional step was performed after the temperature is reached. $30 \mu\text{l}$ of liquid sample were dissolved in 1 ml acetone and analysed via gas chromatography (Shimadzu GC-2010 Plus, FID, Restek Rxi-17Sil column). Calibration of the BT peaks in its different hydrogenation states is described elsewhere³⁷. The gas samples were analysed via gas chromatography with coupled mass spectroscopy (Shimadzu Nexis GC-2030, FID, TCD, HAYESEP N60/80 precolumn, ShinCarbon main column). The calculation of performance parameters conversion, selectivity, degree of hydrogenation as well as molar hydrogen utilization is listed in the supporting information.

reduced initial hydro-generation rate. After approximately 3 h of reaction time, a nearly exponential increase in hydro-generation activity is observed, followed by a slower approach to full conversion state. Although complete conversion is achieved in both cases, the presence of CO significantly delays the overall hydrogenation process, as reflected by a substantially lower DoH of 72.2 %, compared to 97.4 % for pure H_2 . A further increase on CO-content results in a DoH of 6.4 %. In Table 1 is the composition of the C1 components in the gas phase after 6 h reaction time listed. The results support the presence of a parallel reaction pathway by hydrogenation of CO to methane occurring along-side BT hydrogenation⁵⁰. On one hand this additional hydrogen consumption and competition for active sites may contribute to the reduced hydrogenation rate. However, the partial CO-conversion (mainly to methane and in less degree to CO_2) gradually liberates the catalyst surface and makes it available for ongoing BT hydrogenation. The

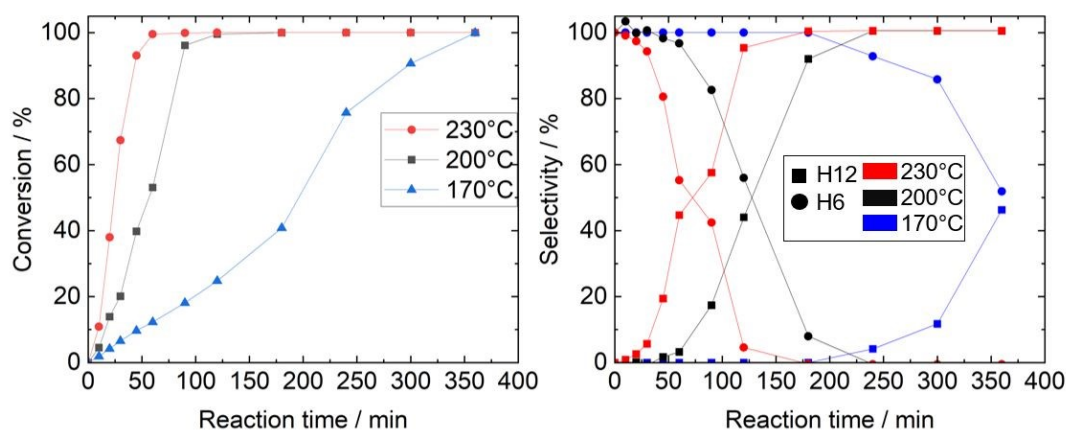


Figure 3 Conversion (left) and selectivity (right) of Benzyltoluene hydrogenation using a commercial Nickel catalyst at 170 °C (blue), 200 °C (black) and 230 °C (red) (reaction conditions: Ni/BT ratio 0.045, $m_{\text{BT}} = 100 \text{ g}$, $t = 6 \text{ h}$; $p = 50 \text{ bar}$, CO-gas fraction 1.2 %)

Results and Discussion

Impact of CO content in hydrogenation gas

A series of experiments was conducted using a $\text{Ni}/\text{Al}_2\text{O}_3/\text{SiO}_2$ catalyst with varying CO content in hydrogen to study its influence on BT conversion and selectivity towards fully hydrogenated H12-BT. CO fractions in the feed gas of 1.2 % and 6 % were adjusted and compared to a CO free benchmark experiment. The results presented in Figure 2 display the conversion (left) and the selectivity (right) for the hydrogenation with different CO concentrations at 170 °C. Comparison of the turnover after 6 h reaction time reveals that a substantially lower conversion of 12.1 % was obtained at a CO gas fraction of 6 %. Nearly all active sites on the catalyst are occupied by competitively adsorbed CO, leading to a pronounced suppression of BT hydrogenation activity. For the experiments without CO and at 1.2 % CO-gas fraction almost full conversion of H0-BT can be achieved after 6 h reaction time. In contrast to the CO-free experiment, the introduction of 1.2 % CO-gas fraction results in a markedly

enhanced hydrogenation rate observed in the experiment with 1.2 % CO gas fraction after 3 h, might be due to reduced CO induced blocking of active sites. Regarding the catalyst stability, no loss of active metal or reduction of surface area could be detected post reaction (See SI Table S2). At the beginning of the reaction, the nickel catalyst is still covered by a superficial oxide layer. It was previously reported that this oxide layer is removed under reaction conditions during the hydrogenation⁵¹. After the reaction, handling of the catalyst under ambient air and subsequent washing, this oxide layer re-forms on the catalyst surface (See SI figure S14 and S15). The H_2 -TPR measurements suggest that the catalyst is present predominantly in its reduced state under the applied reaction conditions, as the observed reduction peaks occur within the temperature window of 150-250 °C, which overlaps with the reaction temperature range (see SI figure S16).

Table 1 Composition of the C1 components of the gas phase of Benzyltoluene hydrogenation using commercial Nickel catalyst without CO impurities, with 1.2 % CO-gas fraction as well as 6 % CO-gas fraction (reaction conditions: Ni/BT ratio 0.045, $m_{\text{BT}} = 100 \text{ g}$, $T = 170 \text{ °C}$, $t = 6 \text{ h}$; $p = 50 \text{ bar}$).

Ratio [%]



	No CO	1.2 % CO	6 % CO
CO	-	13.2	14.5
CH ₄	-	82.4	85.2
CO ₂	-	4.3	0.3

Temperature Variation

The temperature theoretically influences rates of the competitive reactions and the adsorption strength of CO. To investigate these combined effects on hydrogenation performance, temperature variation experiments were conducted. Figure 3 shows BT conversion (left) and selectivity (right) to hydrogenation products at $T = 170\text{ }^{\circ}\text{C}$, $200\text{ }^{\circ}\text{C}$ and $230\text{ }^{\circ}\text{C}$ with 1.2 % CO-content. At $230\text{ }^{\circ}\text{C}$, full conversion was reached after 60 min, while 120 min and 6 h, were required at $200\text{ }^{\circ}\text{C}$ and $170\text{ }^{\circ}\text{C}$, respectively. Consequently, all temperatures allow BT hydrogenation with the Ni-catalyst under presence of CO. While the hydrogenation at $170\text{ }^{\circ}\text{C}$ only displays a DoH of 72.2 %, the other experiments reach full hydrogenation after 4 h at $200\text{ }^{\circ}\text{C}$ and 3 h at $230\text{ }^{\circ}\text{C}$ respectively. CO conversion (see Table 2) of 82.4 % at $170\text{ }^{\circ}\text{C}$ and almost total conversion at $200\text{ }^{\circ}\text{C}$ with 99.6 % and 98.0 % at $230\text{ }^{\circ}\text{C}$ are recorded after 6 h reaction time. At $170\text{ }^{\circ}\text{C}$, as mentioned in the previous chapter, two distinct kinetic regimes can be identified during the reaction. An initial regime characterized by reduced hydrogenation activity is consistent with strong CO co-adsorption and concurrent CO methanation, which limits hydrogen availability and blocks active sites. From an Arrhenius perspective, this behaviour can be attributed to the relatively high apparent activation energy of aromatic BT hydrogenation compared to the lower activation energy associated with CO methanation and the strong temperature dependence of CO adsorption. Table 2 shows the composition of the C1 components in the gas phase after 6 h reaction time. Higher temperatures lead to a pronounced increase in methanation activity, leading to nearly full conversion of CO at $200\text{ }^{\circ}\text{C}$ and $230\text{ }^{\circ}\text{C}$.

Table 2 Composition of the C1 components of the gas phase of Benzyltoluene hydrogenation using a commercial Nickel catalyst at $170\text{ }^{\circ}\text{C}$, $200\text{ }^{\circ}\text{C}$ and $230\text{ }^{\circ}\text{C}$ (reaction conditions: Ni/BT ratio 0.045, $m_{\text{BT}} = 100\text{ g}$, $t = 6\text{ h}$; $p = 50\text{ bar}$, CO-gas fraction 1.2 %)

	Ratio [%]		
	170 °C	200 °C	230 °C
CO	13.2	0.4	1.3
CH ₄	82.4	99.6	98.0
CO ₂	4.3	0	0.8

Schmider *et al.* postulated, that at lower temperatures and high hydrogen partial pressure the hydrogenation of unsaturated compounds is favoured over the otherwise thermodynamically favoured CO methanation on Ni surfaces⁵². Furthermore they reported an increased surface coverage of CO at lower temperatures, leading to site blocking and reduced hydrogen adsorption, which further suppresses methanation as well as the BT conversion in the case of our study⁵². The temperature variation was further conducted with

a CO-content of 6 % and otherwise identical reaction conditions. To get insights into the progression of gas phase composition during the experiment gas samples were taken over the course of the experiment (Figure 4). The respective selectivity plots can be found in the SI (Figure S1-S3).

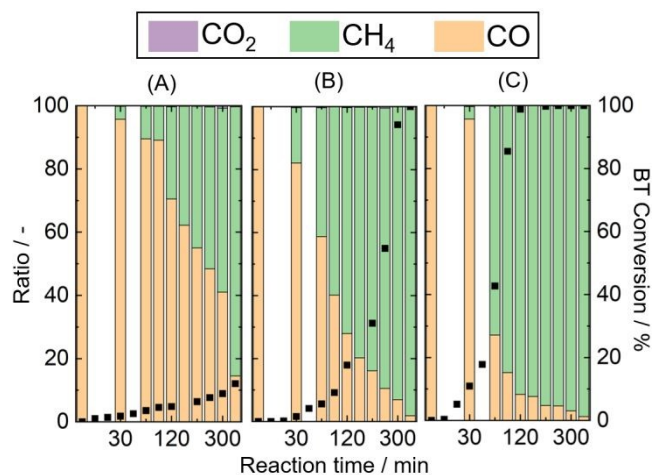


Figure 4 BT Conversion (black) and ratio of the C1 components CO₂ (purple), CH₄ (green) and CO (yellow) of Benzyltoluene hydrogenation using a commercial Nickel catalyst at $170\text{ }^{\circ}\text{C}$ (A), $200\text{ }^{\circ}\text{C}$ (B), $230\text{ }^{\circ}\text{C}$ (C) (reaction conditions: Ni/BT ratio 0.045; $m_{\text{BT}} = 100\text{ g}$, $p = 50\text{ bar}$, $t = 6\text{ h}$, CO-gas fractions 6 %)

At $200\text{ }^{\circ}\text{C}$, complete conversion of H0-BT as well as full hydrogenation were achieved within 6 h of reaction time. Increasing the reaction temperature to $230\text{ }^{\circ}\text{C}$ significantly accelerated the process, with full H0-BT conversion after 3 h and completed hydrogenation to H12-BT after 4 h. In contrast, a conversion of only 12.1 % was reached at $170\text{ }^{\circ}\text{C}$ after 6 h (final DoH of 6.2 %). Nearly complete CO conversion is achieved at $200\text{ }^{\circ}\text{C}$ ($X_{\text{CO}} = 98.1\%$) and $230\text{ }^{\circ}\text{C}$ ($X_{\text{CO}} = 98.9\%$), whereas only 85 % are observed at $170\text{ }^{\circ}\text{C}$. This behaviour can be attributed to accelerated CO methanation kinetics at elevated temperatures, which enhance CO consumption and partially regenerate the catalyst surface⁵³. Furthermore, a temperature of $170\text{ }^{\circ}\text{C}$ seems to be insufficient to provide adequate surface mobility regarding CO desorption, while also being too low to promote sufficient CO methanation to liberate surface centres.

When increasing the CO concentration from 1.2% to 6%, the hydrogenation is markedly inhibited. This inhibitory effect is more pronounced at lower temperatures, where at $200\text{ }^{\circ}\text{C}$ the reaction time increases by 200 % (i.e., the reaction proceeds threefold more slowly), whereas at $230\text{ }^{\circ}\text{C}$ the hydrogenation is only 100% slower (i.e., approximately twofold more slowly). The initial deviation can be attributed to the higher CO concentration, which results in a larger fraction of active sites being blocked by strongly adsorbed CO species. Although the increased temperature accelerates both CO methanation and benzyltoluene hydrogenation, the sustained CO availability maintains a high surface coverage, thereby limiting further improvements in BT conversion despite intrinsically faster hydrogenation kinetics⁵⁴. The subsequent steepening of the conversion profile, after approximately 90 min for the



experiment at 200 °C and after 10 min at 230 °C, reflects partial surface reactivation, reinforcing the conclusion that CO acts as a strong inhibitor by competitively blocking active sites on the nickel surface. At lower CO-partial pressures, CO conversion is limited by gas–liquid mass transfer and competitive adsorption between CO and H₂ on the catalyst surface⁵⁵.

Regarding the catalyst stability, no loss of active metal or reduction of surface area could be detected (See SI Table S2). At the beginning of the reaction, the nickel catalyst is still covered by a superficial oxide layer. It was previously reported that this oxide layer is removed under reaction conditions during the hydrogenation⁵¹. After the reaction, handling of the catalyst under ambient air and subsequent washing, this oxide layer re-forms on the catalyst surface (See SI figure S14 and S15)

Variation of total pressure

Additional experiments at reduced total pressure of 10 bar and 30 bar have been conducted at 200 °C. The CO concentration was kept constant at the beginning of these experiments, while CO partial pressure increased with total pressure accordingly. A decrease in BT conversion was observed with decreasing pressure (Figure 5, selectivity in SI Figure S4-Figure S6). While all experiments reached total conversion of H₀-BT only the 30 bar (DoH ≥ 99.9 % after 6 h) and 50 bar (DoH ≥ 99.9 % after 4 h) experiment achieved full hydrogenation to H₁₂-BT. A DoH of 77.3 % was reached in the 10 bar experiment after 6 h reaction time. Alongside the kinetics of BT conversion, the CO conversion was monitored over the reaction time (Figure 6). About 90 % of CO was converted into methane at all pressures after 30 min of operation. This proves the high activity of the Ni catalysts in the competing methanation reaction. At lower pressures, the CO conversion is influenced by gas–liquid transfer processes or by competitive adsorption between CO and H₂ on the catalyst surface⁵⁵. However, at elevated pressures, where gas solubility and partial pressures are sufficiently high, these effects become less pronounced. Consequently, increasing the total pressure beyond this point does not enhance CO conversion, indicating that the surface reaction kinetics or adsorption equilibrium govern the overall reaction rate under these conditions⁵⁶. CO₂ formation by the reverse water–gas shift reaction could not be observed in the experiments, even though methanation produces water as a stoichiometric byproduct.

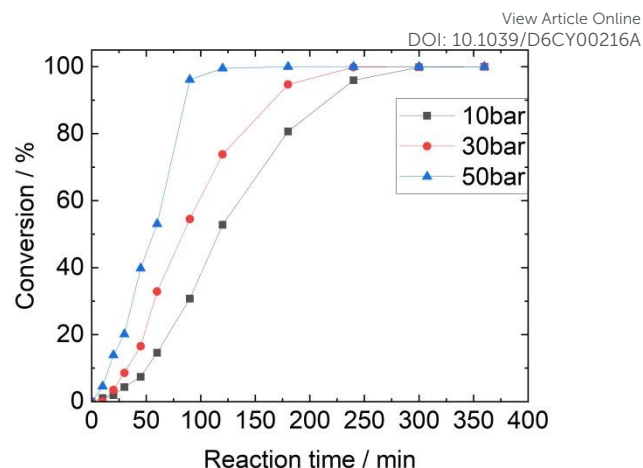


Figure 5 Conversion (left) of Benzyltoluene in hydrogenation using a commercial Nickel catalyst at 10bar (black), 30 bar (red) and 50 bar (blue) (reaction conditions: Ni/BT ratio 0.045; $m_{BT} = 100$ g, $T = 200$ °C, $t = 6$ h, CO-gas fraction 1.2 %)

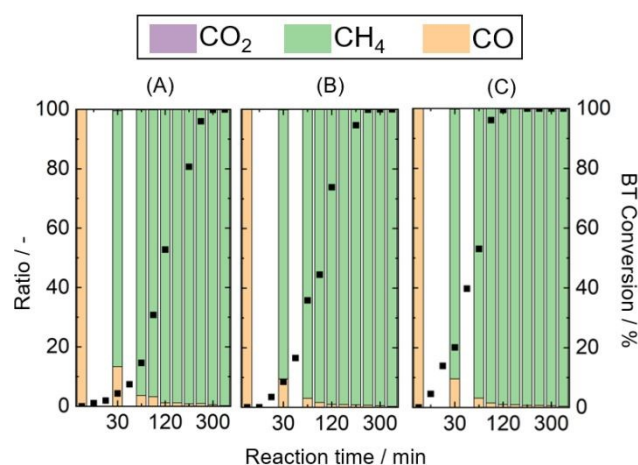


Figure 6 BT Conversion (black) and ratios of the C1 components CO₂ (purple), CH₄ (green) and CO (yellow) of Benzyltoluene hydrogenation using a commercial Nickel catalyst at 10bar (A), 30bar (B) and 50bar (C) (reaction conditions: Ni/BT ratio 0.045; $m_{BT} = 100$ g, $T = 200$ °C, $t = 6$ h, CO-gas fraction 1.2 %)

Hydrogenation with multiple impurities

In a subsequent series of experiments, CO₂ was introduced as an additional gas impurity, to investigate its effect during BT hydrogenation with Ni catalysts. As CO₂ constitutes a major product of biomass gasification alongside hydrogen, its concentration was set to 30 %, in accordance with values reported in literature⁵⁷. This resulted in gas composition of 30 % (15 bar) CO₂, 0.6 % (0.3 bar) CO and 69.4 % (34.7 bar) H₂ at the start of the experiment. The corresponding H₀-BT conversion is presented in Figure 7 (square) at 170 °C and 200 °C and is compared to experiments without CO₂ (Figure 7, triangle) at otherwise identical reaction conditions (Selectivity shown in SI, Figure S7, S8, S11 and S12). For the reference experiments without additional CO₂ full conversion of H₀-BT after 5 h at 170 °C and 3 h at 200 °C was recorded. Additionally, a DoH of 88.4 % was achieved at 170 °C after 6 h while complete hydrogenation was observed after 4 h at 200 °C. The presence of CO₂ had a pronounced negative



impact on the total conversion, resulting in a DoH of only 25.7 % at 170 °C. Raising the temperature only had a minimal effect with an increase of DoH to 32.6 % at 200 °C. The reduced conversion observed upon the addition of CO₂ could be attributed to multiple parallel effects. Dilution of the feed gas lowers the hydrogen partial pressure and thereby reduce the intrinsic BT hydrogenation rate. Beyond this, CO₂ may influence the reaction indirectly through surface-mediated parallel reactions, such as the reverse water–gas shift reaction, resulting in in-situ CO formation and its subsequent competitive adsorption on the catalyst surface. Moreover, while CO₂ binds less strongly than CO, its adsorption can partially occupy active sites, thereby limiting H₂ activation and the hydrogenation of BT⁵⁸. To further assess the role of CO₂, additional experiments were conducted in which the 15 bar CO₂ fraction was replaced by N₂, thereby providing a chemically inert reference to isolate purely dilution-related kinetic effects. The results are shown in Figure 7 (circle). In contrast to the CO₂ experiments, the addition of N₂ results in full conversion after 6 h at 170 °C and after 4 h at 200 °C. Thereby, the DoH reached 62.3 % at 170 °C and 84.0 % at 200 °C, substantially lower than in the experiment with pure hydrogen. The reduced degree of hydrogenation observed in the N₂-diluted experiments can be attributed to the lower hydrogen partial pressure, as nitrogen remains chemically inert⁵⁵. This observation is further substantiated by the gas phase analysis (see Figure 8A), which reveals a substantially slower conversion of CO compared to the reference experiments (See Figure 8C). Since the substitution of CO₂ with N₂ resulted in vastly higher BT conversions, it is assumed that CO₂ in an active compound, competing with H_x-BT for active sites and maybe even participating in parallel reaction. This is further substantiated by the results of the gas phase analysis of the CO₂ substituted experiment (See Figure 8B). CO₂ is gradually converted into methane over the Ni catalyst. Several mechanistic pathways may contribute to this transformation. One possibility is an associative, formate-mediated route, in which CO₂ is first activated on the surface to form *HCOO species, that undergo stepwise hydrogenation via intermediates such as *HCO, *H₂CO, and *CH₃O, ultimately yielding CH₄⁵². Schmitter *et al.* reported that the CH₄ formation via the RWGS pathway is accompanied by an increase in CO partial pressure⁵². In contrast to that, Figure S13 shows the CO content in ppm over the reaction time for the experiment displayed in Figure 8. This indicates that CO did not accumulate in the gas phase to a measurable extent. This observation does not exclude transient CO formation at the catalyst surface, but it suggests that any CO formed was rapidly consumed and did not persist as a detectable gas-phase intermediate. Studies on closely related Ni/SiO₂-Al₂O₃ systems further show that the support composition can significantly affect catalyst performance and CO₂ adsorption behaviour, underlining the relevance of support-dependent CO₂ activation on such Ni-based catalysts^{48,49}. Accordingly, the present experiments do not allow an unambiguous distinction between a direct CO₂ methanation pathway, an associative formate-mediated route, and an RWGS/CO-methanation

sequence involving only transiently formed CO. Nevertheless, independent of the exact mechanistic pathway, CO₂ conversion to methane competes with H_x-BT hydrogenation for hydrogen and catalytically active surface sites, which is consistent with the observed lower hydrogenation rate and reduced DoH.

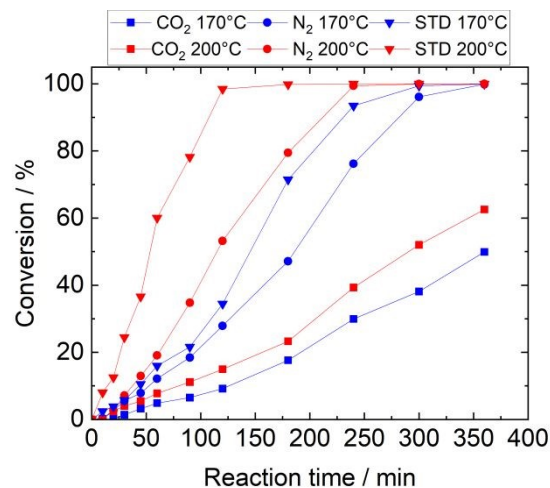


Figure 7 Conversion of Benzyltoluene in hydrogenation using a commercial Nickel catalyst at 170 °C (blue), 200 °C (red) and CO₂ and N₂ as additional gases compared to a hydrogenation experiment with CO as only impurity, (reaction conditions: Ni/BT ratio 0.045; m_{BT} = 100 g, p = 50 bar, p_{N₂/CO₂} = 15 bar, t = 6 h, CO-gas fraction 0,6 %)

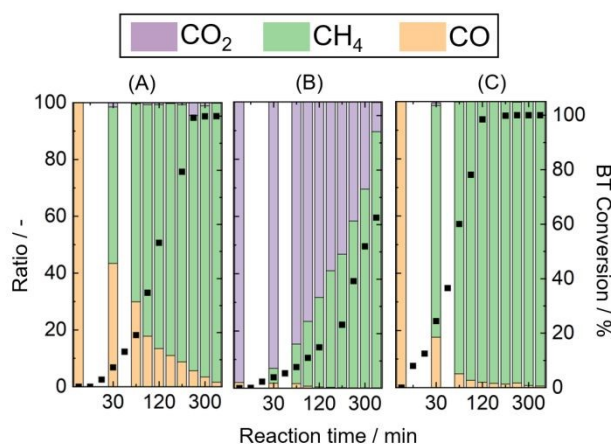


Figure 8 BT Conversion (black) and ratio of the C1 components CO₂ (purple), CH₄ (green) and CO (yellow) in Benzyltoluene hydrogenation using a commercial Nickel catalyst and N₂ (A) and CO₂ (B) as additional gases, compared to a hydrogenation experiment with CO as only impurity (C), (reaction conditions: Ni/BT ratio 0.045; m_{BT} = 100 g, p = 50 bar, p_{N₂/CO₂} = 15 bar, T = 200 °C, t = 6 h, CO-gas fraction 0,6 %)

Hydrogen utilization

Another important consideration is the degree of hydrogen utilization towards the desired purification reaction. Complete hydrogenation of 100 g H₀-BT requires 3.29 mol H₂, whereas methanation of 0.3 bar CO (corresponding to a 0.6 % CO-gas fraction at 50 bar total pressure) consumes only 4.89×10⁻³ mol H₂. This corresponds to a hydrogen utilization of 99.86 % with respect to the purification step. An increase in CO content to 0.6 bar (corresponding to 1.2 % CO-gas fraction at



50 bar) consumes 9.2×10^{-3} mol H_2 with a utilization degree of 99.72 %. The highest CO partial pressure in this work was 3 bar (corresponding to 6.0 % CO-gas fraction at 50 bar) and consumed 4.89×10^{-2} mol H_2 , corresponding to a utilization degree of 98.54 %. These results indicate that hydrogen losses due to CO methanation are negligible at such low CO concentrations in hydrogen and that the observed acceleration in reaction rate is primarily associated with the removal of CO as a strongly adsorbed catalyst inhibitor, leading to progressive reactivation of the nickel surface. In comparison, the addition of 15 bar CO_2 leads to the consumption of 0.31 mol H_2 during the methanation reaction, reducing the utilization degree to 90.6 %. It should be noted, however, that the resulting gas stream constitutes an energy-rich, combustible mixture that can be valorized in downstream processes, offering a potential route for energy recovery that is not available in the original CO_2/CO feed impurities. In Summary while Ni displays the clear advantages including low material cost and the absence of irreversible deactivation by CO or CO_2 due to their conversion via methanation, which continuously regenerates active surface sites. This behavior represents a limitation for mixed-gas hydrogenation of the LOHC benzyltoluene, as methanation is associated with hydrogen consumption, particularly in gas mixtures containing high concentrations of CO and/or CO_2 . Consequently, for typical biomass-derived gas mixtures, an upstream CO_2 removal step is necessary to significantly reduce the CO_2 concentration prior to hydrogenation. From a process-engineering perspective, this requirement is realistic because upstream CO_2 removal is already an established unit operation in industrial hydrogen and syngas processing, with amine scrubbing, physical-solvent absorption, and Pressure swing adsorption-based (PSA) polishing representing the most relevant options in this context^{59,60}. For H_2 -rich shifted syngas, MDEA-based amine scrubbing is widely used and reported to achieve roughly 90–99.8 % CO_2 capture, depending on process design and optimization⁶¹. Applied to the feed composition in this study (containing 30 vol% CO_2), such capture levels would lower the residual CO_2 concentration to approximately 3.0 vol% at 90 % and up to 0.06 vol% at 99.8 % capture rate. However, deeper capture is associated with higher solvent-regeneration duty, additional CO_2 compression work, and larger absorber/stripper equipment⁶¹. In the optimized MDEA process reported by Antonini *et al.*, the specific equivalent work increased from about $0.585 \text{ MJ kg}_{CO_2}^{-1}$ at 90 % capture to about $0.681 \text{ MJ kg}_{CO_2}^{-1}$ at 99.8 % capture, while feasible packed-column designs remained below 15 m packing height but increased substantially toward deeper capture⁶¹. For pressurized syngas, physical solvents such as Selexol or Rectisol are attractive alternatives for bulk CO_2 removal because they perform well at elevated CO_2 partial pressure and generally require less thermal regeneration than chemical solvents, although they are less suitable for very deep polishing^{62,63}. PSA, in contrast, is widely used as a final hydrogen purification step in biomass-to-hydrogen process chains, but is less attractive as the sole front-end option for a stream containing higher CO_2 content⁶⁰. In this context, the practical potential of the investigated Ni catalysts lies in

process chains in which CO_2 is removed upstream while residual CO remains, since the present results show substantially stronger inhibition by 30 vol% CO_2 than by 1.2 vol% CO. The corresponding limitation is that the economic advantage of cheap commercial Ni- catalyst may be partly offset if very deep CO_2 removal is required to suppress the pronounced CO_2 -induced loss in hydrogenation performance, because deeper capture is associated with higher regeneration energy, additional CO_2 compression duty, and larger absorber/stripper equipment⁶¹.

Conclusion

In this study a commercially available Ni catalyst was investigated regarding its activity in benzyltoluene (BT) hydrogenation with impure hydrogen, containing CO (0.6–6 % gas fraction), as well as CO_2 (30 % gas fraction). These were chosen as relevant impurities in biomass-derived hydrogen and being known to kinetically inhibit typical noble metal hydrogenation catalysts. CO strongly affected H0-BT conversion and degree of hydrogenation. Whereas complete conversion was still achieved in the absence of CO and at 1.2 vol% CO, although with delayed kinetics and reduced selectivity due to competitive adsorption and parallel CO methanation, 6 vol% CO led to severe inhibition and a pronounced suppression of hydrogenation activity. Additional temperature- and pressure-dependent experiments showed that CO inhibition is largely reversible and governed by surface kinetics. Increasing temperature promoted CO conversion and catalyst surface reactivation, while lowering the pressure from the standard condition of 50 bar reduced H0-BT hydrogenation performance. Since hydrogen consumption by CO methanation remained negligible in the overall balance, the detrimental effect of CO is mainly attributed to temporary blocking of active sites rather than to a substantial loss of hydrogen. In contrast, CO_2 caused a much stronger deterioration in H0-BT hydrogenation performance. Besides competitive adsorption, the parallel methanation of CO_2 reduced the hydrogen available for Hx-BT hydrogenation and thereby significantly lowered the final degree of hydrogenation and hydrogen utilization. Comparison with N_2 -containing reference experiments confirmed that the inhibitory effect of CO_2 cannot be explained by simple dilution alone. Overall, the results demonstrate that Ni catalysts are promising for LOHC-based purification of CO-containing hydrogen streams, while effective upstream CO_2 removal remains necessary for CO_2 -rich biomass-derived feeds.

In conclusion nickel catalysts combine low cost with resistance to irreversible CO/ CO_2 poisoning due to continuous surface regeneration via methanation; however, this advantage becomes a limitation in mixed-gas hydrogenation because methanation preferentially consumes hydrogen, especially at high CO/ CO_2 levels. Therefore, biomass-derived gas streams require upstream CO_2 removal, for example by amine scrubbing, to enable efficient hydrogenation.



Author contributions

LP: Data curation, formal analysis, investigation, methodology, visualization, conceptualization, writing – original draft. PS: Conceptualization, project administration, supervision

Conflicts of interest

There are no conflicts to declare

Data availability

Data for this article is available at the data repository zenodo (10.5281/zenodo.18656400)

Acknowledgements

The authors would like to thank the Federal Ministry of Research, Technology, and Space for funding the BMFTR Junior Research Group FAIR-H2 (grant number FKZ: 03SF0730)

Notes and references

Abbreviations: BT: benzyltoluene H0-BT: fully dehydrogenated benzyltoluene, H_x-BT: partially hydrogenated benzyltoluene, *X: substance X adsorbed on the catalyst surface; DoH: degree of hydrogenation, H6: Partially hydrogenated benzyltoluene with a DoH of exactly 50 %, H12: fully hydrogenated benzyltoluene

References

- (1) Tavares Borges, P.; Silva Lora, E. E.; Venturini, O. J.; Errera, M. R.; Yepes Maya, D. M.; Makarfi Isa, Y.; Kozlov, A.; Zhang, S. A Comprehensive Technical, Environmental, Economic, and Bibliometric Assessment of Hydrogen Production Through Biomass Gasification, Including Global and Brazilian Potentials. *Sustainability* **2024**, *16* (21), 9213. <https://doi.org/10.3390/su16219213>.
- (2) Dasappa, S.; Shivapuji, A. M.; Stanislaus, M. S. Green Hydrogen from Biomass Through Gasification—A Carbon Negative Route for Hydrogen Production. In *Climate Action and Hydrogen Economy: Technologies Shaping the Energy Transition*; Goel, M., Sen, G., Eds.; Springer Nature Singapore: Singapore, 2024; pp 175–194. https://doi.org/10.1007/978-981-99-6237-2_11.
- (3) Alptekin, F. M.; Celiktas, M. S. Review on Catalytic Biomass Gasification for Hydrogen Production as a Sustainable Energy Form and Social, Technological, Economic, Environmental, and Political Analysis of Catalysts. *ACS Omega* **2022**, *7* (29), 24918–24941. <https://doi.org/10.1021/acsomega.2c01538>.
- (4) Full, J.; Merseburg, S.; Miede, R.; Sauer, A. A New Perspective for Climate Change Mitigation—Introducing Carbon-Negative Hydrogen Production from Biomass with Carbon Capture and Storage (HyBECCS). *Sustainability* **2021**, *13* (7), 4026. <https://doi.org/10.3390/su13074026>.
- (5) Kundu, P.; Vineetha, S. V.; Mohan, A.; Ravikumar, A. Bio-Hydrogen Production from Various Waste Resources through Circular Economy: Current Technologies and Future Perspective. *J. Mater. Cycles Waste Manag.* **2025**, *27* (3), 1263–1282. <https://doi.org/10.1007/s10163-025-02183-x>.
- (6) Abawalo, M.; Pikoń, K.; Landrat, M. Comparative Life Cycle Assessment of Hydrogen Production via Biogas Reforming and Agricultural Residue Gasification. *Appl. Sci.* **2025**, *15* (9), 5029. <https://doi.org/10.3390/app15095029>.
- (7) Rosa, L.; Mazzotti, M. Potential for Hydrogen Production from Sustainable Biomass with Carbon Capture and Storage. *Renew. Sustain. Energy Rev.* **2022**, *157*, 112123. <https://doi.org/10.1016/j.rser.2022.112123>.
- (8) Khlifi, S.; Pozzobon, V.; Lajili, M. A Comprehensive Review of Syngas Production, Fuel Properties, and Operational Parameters for Biomass Conversion. *Energies* **2024**, *17* (15), 3646. <https://doi.org/10.3390/en17153646>.
- (9) Gebresilasie, T. N.; Belete, F. A.; Mekonen, A. G.; Kahsay, K. F.; Abraha, S. K. Simulation Based Analysis of Syngas Production from Combined Solid Waste Biomass of Rice Husk Coffee Husk and Sawdust. *Discov. Energy* **2025**, *5* (1), 25. <https://doi.org/10.1007/s43937-025-00093-5>.
- (10) Gao, Y.; Wang, M.; Raheem, A.; Wang, F.; Wei, J.; Xu, D.; Song, X.; Bao, W.; Huang, A.; Zhang, S.; Zhang, H. Syngas Production from Biomass Gasification: Influences of Feedstock Properties, Reactor Type, and Reaction Parameters. *ACS Omega* **2023**, *8* (35), 31620–31631. <https://doi.org/10.1021/acsomega.3c03050>.
- (11) Faddeev, N.; Belichenko, M.; Kuriganova, A.; Smirnova, N. Carbon Monoxide Poisoning and Mitigation Strategies for Platinum Catalysts Prepared via Pulse Alternating Current Technique. *J. Electrochem. Sci. Technol.* **2025**, *16* (3), 304–313. <https://doi.org/10.33961/jecst.2024.01032>.
- (12) Chen, W.; Cao, J.; Fu, W.; Zhang, J.; Qian, G.; Yang, J.; Chen, D.; Zhou, X.; Yuan, W.; Duan, X. Molecular-Level Insights into the Notorious CO

View Article Online
DOI: 10.1039/D5CY00216A



- Poisoning of Platinum Catalyst. *Angew. Chem. Int. Ed.* **2022**, *61* (16).
<https://doi.org/10.1002/anie.202200190>.
- (13) Dong, A.-Q.; Li, H.; Wu, H.-M.; Li, K.-X.; Shao, Y.-K.; Li, Z.-G.; Sun, S.-H.; Wang, W.-C.; Hu, W.-B. Weakening CO Poisoning over Size- and Support-Dependent Pt_n/X-Graphene Catalyst (X = C, B, N, n = 1–6, 13). *Rare Met.* **2023**, *42* (4), 1138–1145.
<https://doi.org/10.1007/s12598-022-02210-y>.
- (14) Ni, W.; Wang, T.; Héroguel, F.; Krammer, A.; Lee, S.; Yao, L.; Schüler, A.; Luterbacher, J. S.; Yan, Y.; Hu, X. An Efficient Nickel Hydrogen Oxidation Catalyst for Hydroxide Exchange Membrane Fuel Cells. *Nat Mater* **2022**, *21*, 804–810.
<https://doi.org/10.1038/s41563-022-01221-5>.
- (15) Katsumi, T.; Noguchi, H.; Zemba, A.; Sato, D.; Kadowaki, S. The Effects of Initial Temperature and Inert-Gas Addition on the Dynamic Characteristics of Hydrogen–Air Deflagration. *J. Vis.* **2025**, *28* (2), 291–301.
<https://doi.org/10.1007/s12650-024-01040-7>.
- (16) Navarro-Cárdenas, I.; Martín, Á. Thermodynamic Modelling of Mixtures of Water, Carbon Dioxide and Hydrogen at High Pressure and Temperature for Hydrothermal CO₂ Reduction Processes. *Front. Phys.* **2023**, *11*, 1219630.
<https://doi.org/10.3389/fphy.2023.1219630>.
- (17) Kim, G.; Lee, H. Developing Heterogeneous Catalysts for Reverse Water–Gas Shift Reaction in CO₂ Valorization. *Korean J. Chem. Eng.* **2025**, *42* (13), 3101–3112.
<https://doi.org/10.1007/s11814-024-00349-1>.
- (18) Martinez-Boggio, S. D.; Merola, S. S.; Teixeira Lacava, P.; Irimescu, A.; Curto-Risso, P. L. Effect of Fuel and Air Dilution on Syngas Combustion in an Optical SI Engine. *Energies* **2019**, *12* (8), 1566.
<https://doi.org/10.3390/en12081566>.
- (19) Nguyen, M. T.; Bui, V. G.; Do, H.-Q.; Do, P. N.; Nguyen, X. B.; Ho, T. T.; Ho, T. N. A. Effect of Hydrogen-Enriched Syngas and Nitrogen Dilution on Ammonia Deflagration Characteristics at Moderate Pressure. *ACS Omega* **2025**, *10* (25), 27404–27414.
<https://doi.org/10.1021/acsomega.5c03002>.
- (20) Cavaliere, P. Hydrogen Separation and Purification. In *Water Electrolysis for Hydrogen Production*; Cavaliere, P., Ed.; Springer International Publishing: Cham, 2023; pp 509–541. https://doi.org/10.1007/978-3-031-37780-8_14.
- (21) Burgers, I.; Dehdari, L.; Xiao, P.; Li, K. G.; Goetheer, E.; Webley, P. Techno-Economic Analysis of PSA Separation for Hydrogen/Natural Gas Mixtures at Hydrogen Refuelling Stations. *Int. J. Hydrog. Energy* **2022**, *47* (85), 36163–36174.
<https://doi.org/10.1016/j.ijhydene.2022.08.175>.
- (22) Du, Z.; Liu, C.; Zhai, J.; Guo, X.; Xiong, Y.; Su, W.; He, G. A Review of Hydrogen Purification Technologies for Fuel Cell Vehicles. *Catalysts* **2021**, *11* (3), 393.
<https://doi.org/10.3390/catal11030393>.
- (23) Abdul Muin, N. A.; Nwaha Isah, A.; Asli, U. A.; Sadikin, A. N.; Norazahar, N.; Kamaruddin, M. J.; Hassim, M. H.; Wai Shin, H.; Azman, N. R. A Short Review on Various Purification Techniques Suitable for Biohydrogen-Mixed Gases. *J. Energy Saf. Technol. JEST* **2021**, *3* (2).
<https://doi.org/10.11113/jest.v3n2.52>.
- (24) Kim, Y.; Yang, H. Hydrogen Purity: Influence of Production Methods, Purification Techniques, and Analytical Approaches. *Energies* **2025**, *18* (3), 741.
<https://doi.org/10.3390/en18030741>.
- (25) Król, A.; Gajec, M.; Holewa-Rataj, J.; Kukulska-Zajac, E.; Rataj, M. Hydrogen Purification Technologies in the Context of Its Utilization. *Energies* **2024**, *17* (15), 3794.
<https://doi.org/10.3390/en17153794>.
- (26) Naeiji, E.; Noorpoor, A.; Ghanavati, H. Energy, Exergy, and Economic Analysis of Cryogenic Distillation and Chemical Scrubbing for Biogas Upgrading and Hydrogen Production. *Sustainability* **2022**, *14* (6), 3686.
<https://doi.org/10.3390/su14063686>.
- (27) Krótki, A.; Bigda, J.; Spietz, T.; Ignasiak, K.; Matusiak, P.; Kowol, D. Performance Evaluation of Pressure Swing Adsorption for Hydrogen Separation from Syngas and Water–Gas Shift Syngas. *Energies* **2025**, *18* (8), 1887.
<https://doi.org/10.3390/en18081887>.
- (28) Bong, B.; Mebrahtu, C.; Jurado, D.; Bösmann, A.; Wasserscheid, P.; Palkovits, R. Hydrogen Loading and Release Potential of the LOHC System Benzyltoluene/Perhydro Benzyltoluene over S–Pt/TiO₂ Catalyst. *ACS Eng. Au* **2024**, *4* (3), 359–367.
<https://doi.org/10.1021/acseengineeringau.4c00003>.
- (29) Bong, B.; Kopp, W. A.; Nevolianis, T.; Mebrahtu, C.; Leonhard, K.; Palkovits, R. Reaction Equilibria in the Hydrogen Loading and Release of the LOHC System Benzyltoluene/Perhydro Benzyltoluene.



- Chem. Eng. Technol.* **2025**, *48* (3), e12002. <https://doi.org/10.1002/ceat.12002>.
- (30) Mahayni, Y.; Maurer, L.; Auer, F.; Hutzler, A.; Wasserscheid, P.; Wolf, M. Structure Sensitivity of the Low-Temperature Dehydrogenation of Perhydro Dibenzyltoluene on Supported Platinum Nanoparticles. *Catal. Sci. Technol.* **2024**, *14* (18), 5464–5473. <https://doi.org/10.1039/D4CY00032C>.
- (31) Alconada, K.; Mariño, F.; Agirre, I.; Barrio, V. L. Exploring Perhydro-Benzyltoluene Dehydrogenation Using Sulfur-Doped PtMo/Al₂O₃ Catalysts. *Catalysts* **2025**, *15* (5), 485. <https://doi.org/10.3390/catal15050485>.
- (32) Rüde, T.; Lu, Y.; Anschütz, L.; Blasius, M.; Wolf, M.; Preuster, P.; Wasserscheid, P.; Geißelbrecht, M. Performance of Continuous Hydrogen Production from Perhydro Benzyltoluene by Catalytic Distillation and Heat Integration Concepts with a Fuel Cell. *Energy Technol.* **2023**, *11* (3), 2201366. <https://doi.org/10.1002/ente.202201366>.
- (33) Jorschick, H. Ein-Reaktor-Konzept und Mischgashydrierung als Verfahrensvarianten zur Effizienzsteigerung in der LOHC-basierten Wasserstoffspeicherung. Dissertation, Friedrich-Alexander-Universität Erlangen-Nürnberg, Erlangen, 2019.
- (34) Inagawa, K.; Matsumura, D.; Taniguchi, M.; Uegaki, S.; Nakayama, T.; Urano, J.; Aotani, T.; Tanaka, H. Development of Hydrogen Oxidation Reaction Catalysts to Overcome CO Poisoning and Elucidation of Reaction Mechanism. *J. Phys. Chem. C* **2023**, *127* (24), 11542–11549. <https://doi.org/10.1021/acs.jpcc.3c02237>.
- (35) Niermann, M.; Drünert, S.; Kaltschmitt, M.; Bonhoff, K. Liquid Organic Hydrogen Carriers (LOHCs) – Techno-Economic Analysis of LOHCs in a Defined Process Chain. *Energy Environ. Sci.* **2019**, *12* (1), 290–307. <https://doi.org/10.1039/C8EE02700E>.
- (36) Kerscher, M.; Jander, J. H.; Cui, J.; Maurer, L. A.; Wolf, P.; Hofmann, J. D.; Köksal, A.; Zachskorn, H.; Auer, F.; Schulz, P. S.; Wasserscheid, P.; Rausch, M. H.; Koller, T. M.; Fröba, A. P. Thermophysical Properties of the Liquid Organic Hydrogen Carrier System Based on Benzyltoluene Considering Influences of Isomerism and Dissolved Hydrogen. *Int. J. Hydrog. Energy* **2024**, *77*, 1009–1025. <https://doi.org/10.1016/j.ijhydene.2024.06.131>.
- (37) Rüde, T.; Dürr, S.; Preuster, P.; Wolf, M.; Wasserscheid, P. Benzyltoluene/Perhydro Benzyltoluene – Pushing the Performance Limits of Pure Hydrocarbon Liquid Organic Hydrogen Carrier (LOHC) Systems. *Sustain. Energy Fuels* **2022**, *6* (6), 1541–1553. <https://doi.org/10.1039/D1SE01767E>.
- (38) Jorschick, H.; Vogl, M.; Preuster, P.; Bösmann, A.; Wasserscheid, P. Hydrogenation of Liquid Organic Hydrogen Carrier Systems Using Multicomponent Gas Mixtures. *Int. J. Hydrog. Energy* **2019**, *44* (59), 31172–31182. <https://doi.org/10.1016/j.ijhydene.2019.10.018>.
- (39) Sheng, Y.; Seitz, A.; Gambu, T.; Zhang, K.; Schühle, P.; Retzer, T. Site Blocking Effects on P-Modified Pd/Al₂O₃ Catalysts for LOHC Hydrogenation: An *In Situ* DRIFTS Study. *Catal. Sci. Technol.* **2025**, *15* (11), 3423–3433. <https://doi.org/10.1039/D4CY01456A>.
- (40) Wang, R.; Zhang, M.; Zhang, J.; Yang, J. Supported Nickel-based Catalysts for Heterogeneous Hydrogenation of Aromatics. *ChemistrySelect* **2023**, *8* (45), e202302787. <https://doi.org/10.1002/slct.202302787>.
- (41) Wang, Z.; Dong, C.; Tang, X.; Qin, X.; Liu, X.; Peng, M.; Xu, Y.; Song, C.; Zhang, J.; Liang, X.; Dai, S.; Ma, D. CO-Tolerant RuNi/TiO₂ Catalyst for the Storage and Purification of Crude Hydrogen. *Nat. Commun.* **2022**, *13* (1), 4404. <https://doi.org/10.1038/s41467-022-32100-x>.
- (42) Sekine, H.; Ohshima, M.; Kurokawa, H.; Miura, H. Liquid Phase Hydrogenation of Naphthalene in the Presence of CO over Supported Ni Catalyst. *React. Kinet. Catal. Lett.* **2008**, *95* (1), 99–105. <https://doi.org/10.1007/s11144-008-5295-5>.
- (43) Le, T. A.; Kang, J. K.; Park, E. D. Active Ni/SiO₂ Catalysts with High Ni Content for Benzene Hydrogenation and CO Methanation. *Appl. Catal. Gen.* **2019**, *581*, 67–73. <https://doi.org/10.1016/j.apcata.2019.05.020>.
- (44) Gao, J.; Jia, C.; Li, J.; Zhang, M.; Gu, F.; Xu, G.; Zhong, Z.; Su, F. Ni/Al₂O₃ Catalysts for CO Methanation: Effect of Al₂O₃ Supports Calcined at Different Temperatures. *J. Energy Chem.* **2013**, *22* (6), 919–927. [https://doi.org/10.1016/S2095-4956\(14\)60273-4](https://doi.org/10.1016/S2095-4956(14)60273-4).
- (45) Riani, P.; Spennati, E.; Garcia, M. V.; Escribano, V. S.; Busca, G.; Garbarino, G. Ni/Al₂O₃ Catalysts for CO₂ Methanation: Effect of Silica and Nickel Loading. *Int. J. Hydrog. Energy* **2023**, *48* (64),



- 24976–24995.
<https://doi.org/10.1016/j.ijhydene.2023.01.002>.
- (46) Italiano, C.; Llorca, J.; Pino, L.; Ferraro, M.; Antonucci, V.; Vita, A. CO and CO₂ Methanation over Ni Catalysts Supported on CeO₂, Al₂O₃ and Y₂O₃ Oxides. *Appl. Catal. B Environ.* **2020**, *264*, 118494.
<https://doi.org/10.1016/j.apcatb.2019.118494>.
- (47) Ju Jung, H.; Jeong, H.; Kim, D.; Ko, H.; Bo Han, G.; Jeong, B.; Wan Kim, T.; Suh, Y.-W. Metal–Support Interface Engineering of Ni Catalysts for Improved H₂ Storage Performance: Grafting Alkyltriethoxysilane onto Commercial Alumina. *Chem. Eng. J.* **2023**, *469*, 143872.
<https://doi.org/10.1016/j.cej.2023.143872>.
- (48) Riani, P.; Valsamakis, I.; Cavattoni, T.; Sanchez Escribano, V.; Busca, G.; Garbarino, G. Ni/SiO₂-Al₂O₃ Catalysts for CO₂ Methanation: Effect of La₂O₃ Addition. *Appl. Catal. B Environ.* **2021**, *284*, 119697.
<https://doi.org/10.1016/j.apcatb.2020.119697>.
- (49) Vrijburg, W. L.; Garbarino, G.; Chen, W.; Parastaev, A.; Longo, A.; Pidko, E. A.; Hensen, E. J. M. Ni-Mn Catalysts on Silica-Modified Alumina for CO₂ Methanation. *J. Catal.* **2020**, *382*, 358–371.
<https://doi.org/10.1016/j.jcat.2019.12.026>.
- (50) Wodołański, A. Modelling of Carbon Monoxide and Carbon Dioxide Methanation under Industrial Condition. In *Biogas - Recent Advances and Integrated Approaches*; El-Fatah Abomohra, A., Elsayed, M., Qin, Z., Ji, H., Liu, Z., Eds.; IntechOpen, 2021.
<https://doi.org/10.5772/intechopen.85170>.
- (51) Tricker, A. W.; Najmi, S.; Phillips, E. V.; Hebisch, K. L.; Kang, J. X.; Sievers, C. Mechanocatalytic Hydrogenolysis of Benzyl Phenyl Ether over Supported Nickel Catalysts. *RSC Sustain.* **2023**, *1* (2), 346–356.
<https://doi.org/10.1039/D2SU00089J>.
- (52) Schmider, D.; Maier, L.; Deutschmann, O. Reaction Kinetics of CO and CO₂ Methanation over Nickel. *Ind. Eng. Chem. Res.* **2021**, *60* (16), 5792–5805.
<https://doi.org/10.1021/acs.iecr.1c00389>.
- (53) Rostrup-Nielsen, J. R. Catalytic Steam Reforming. In *Catalysis: Science and Technology Volume 5*; Anderson, J. R., Boudart, M., Eds.; Springer Berlin Heidelberg: Berlin, Heidelberg, 1984; pp 1–117.
https://doi.org/10.1007/978-3-642-93247-2_1.
- (54) Wei, J.; Iglesia, E. Mechanism and Site Requirements for Activation and Chemical Conversion of Methane on Supported Pt Clusters and Turnover Rate Comparisons among Noble Metals. *J. Phys. Chem. B* **2004**, *108* (13), 4094–4103. <https://doi.org/10.1021/jp036985z>. DOI: 10.1039/D6GY00216A
- (55) Kim, W.; Kamal, K. M.; Seo, D. J.; Yoon, W. L. Kinetic Study on CO-Selective Methanation over Nickel-Based Catalysts for Deep Removal of CO from Hydrogen-Rich Reformate. *Catalysts* **2021**, *11* (12), 1429.
<https://doi.org/10.3390/catal11121429>.
- (56) Yue, Y.; Wang, T.; Sakai, M.; Shen, Y. Particle-Scale Study of Spout Deflection in a Flat-Bottomed Spout Fluidized Bed. *Chem. Eng. Sci.* **2019**, *205*, 121–133.
<https://doi.org/10.1016/j.ces.2019.04.031>.
- (57) Cay, H.; Duman, G.; Yanik, J. Two-Step Gasification of Biochar for Hydrogen-Rich Gas Production: Effect of the Biochar Type and Catalyst. *Energy Fuels* **2019**, *33* (8), 7398–7405.
<https://doi.org/10.1021/acs.energyfuels.9b01354>.
- (58) Nielsen, N. D.; Jensen, A. D.; Christensen, J. M. The Roles of CO and CO₂ in High Pressure Methanol Synthesis over Cu-Based Catalysts. *J. Catal.* **2021**, *393*, 324–334.
<https://doi.org/10.1016/j.jcat.2020.11.035>.
- (59) Jansen, D.; Gazzani, M.; Manzolini, G.; Dijk, E. V.; Carbo, M. Pre-Combustion CO₂ Capture. *Int. J. Greenh. Gas Control* **2015**, *40*, 167–187.
<https://doi.org/10.1016/j.ijggc.2015.05.028>.
- (60) Lundgren, J.; Vreugdenhil, B.; Gynjkanlou, Y.; Baldwin, R. *Biomass Gasification for Hydrogen Production*; IEA Bioenergy, 2025.
https://www.ieabioenergy.com/wp-content/uploads/2025/03/IEA-Bioenergy_T33_Bio-H2_Final_v2.pdf.
- (61) Antonini, C.; Pérez-Calvo, J.-F.; Van Der Spek, M.; Mazzotti, M. Optimal Design of an MDEA CO₂ Capture Plant for Low-Carbon Hydrogen Production — A Rigorous Process Optimization Approach. *Sep. Purif. Technol.* **2021**, *279*, 119715.
<https://doi.org/10.1016/j.seppur.2021.119715>.
- (62) Jansen, D.; Gazzani, M.; Manzolini, G.; Dijk, E. V.; Carbo, M. Pre-Combustion CO₂ Capture. *Int. J. Greenh. Gas Control* **2015**, *40*, 167–187.
<https://doi.org/10.1016/j.ijggc.2015.05.028>.
- (63) N. Borhani, T.; Wang, M. Role of Solvents in CO₂ Capture Processes: The Review of Selection and Design Methods. *Renew. Sustain. Energy Rev.* **2019**, *114*, 109299.
<https://doi.org/10.1016/j.rser.2019.109299>.



Data for this article is available at the data repository zenodo (10.5281/zenodo.18656400)

View Article Online
DOI: 10.1039/D6CY00216A

Open Access Article. Published on 16 April 2026. Downloaded on 4/17/2026 8:04:30 AM.
This article is licensed under a Creative Commons Attribution 3.0 Unported Licence.

